

Phase Coherence Analysis of Solar Magnetic Activity

Carl J. Henney and John W. Harvey

*National Solar Observatory**, Tucson, Arizona, 85726-6732, USA

Abstract.

Over 24 years of synoptic data from the NSO Kitt Peak Vacuum Telescope is used to investigate the coherency and source of the 27-day (synodic) periodicity that is observed over multiple solar cycles in various solar-related time series. A strong 27.03-day period signal, recently reported by Neugebauer et al. (2000), is clearly detected in power spectra of time series from integrated full-disk measurements of the magnetic flux in the 868.8 nm Fe I line and the line equivalent width in the 1083.0 nm He I line. Using spectral analysis of synoptic maps of photospheric magnetic fields, in addition to constructing maps of the surface distribution of activity, we find that the origin of the 27.03-day signal is long-lived complexes of active regions in the northern hemisphere at a latitude of approximately 18 degrees. In addition, using a new time series analysis technique which utilizes the phase variance of a signal, the coherency of the 27.03-day period signal is found to be significant for the past two decades. However, using the past 120 years of the sunspot number time series, the 27.03-day period signal is found to be a short-lived, no longer than two 11-year solar cycles, quasi-stationary signal.

1. Introduction

The variability of solar magnetic activity, along with differential rotation and meridional flow, leads to a spatially and temporally dynamic solar surface. With such continuous change, the temporal coherence of observed solar magnetic activity is expected to decrease for intervals much greater than the average lifetime of an active region. Thus one might expect only a broad peak covering the range of rotation periods in spectral analysis of solar activity time series. However, the persistence of specific 27-day periodicities (all periods stated in this paper are synodic) over several solar cycles found in various solar related time series has led to numerous papers supporting the existence of preferred longitudes of solar magnetic activity (e.g. Svalgaard and Wilcox, 1975; Bogart, 1982; Balthasar and Schüssler, 1983; Neugebauer et al., 2000). Svalgaard and Wilcox (1975) reported a periodicity near 27-days that lasted over five solar cycles using autocorrelation analysis of interplanetary magnetic field data. Bogart (1982) revealed a persistent 27.5 ± 0.5 day period signal using spectral and autocorrelation analysis

* National Solar Observatory (NSO) is operated by the Association of Universities for Research in Astronomy (AURA, Inc.) under cooperative agreement with the National Science Foundation (NSF).



with 128 years of the sunspot number time series. In addition, correlating sunspot group longitudinal positions with high speed solar wind, Balthasar and Schüssler (1983) also found a persistent periodicity at 27.0-days.

Using spectral analysis of low-resolution photospheric magnetic field observations from the Wilcox Solar Observatory (WSO) during solar cycle 21, Hoeksema and Scherrer (1987) and Antonucci, Hoeksema, and Scherrer (1990) found asymmetrical rotation periods of 26.9 and 28.1 days for the northern and southern hemispheres respectively. Combining solar flare observations by hemisphere, asymmetrical rotation rates are also detected for prominent flare activity regions, with periods of 26.72 and 27.99 days for the northern and southern hemispheres respectively (Bai, 1990). Using solar wind velocity data from 1964 through 1975, Gosling et al. (1977) reported a pronounced modulation at 27.025 days. Recent work by Neugebauer et al. (2000) using over three decades of solar magnetic field and solar wind data, demonstrated a very persistent signal with a well-defined period of 27.03 ± 0.02 days. They used the difference between the maximum and minimum amplitudes of time averaged values, binned in solar longitude for a band of rotational periods, to select coherent signals. The longevity of the signal over several solar cycles suggests a fixed longitudinal magnetic structure in the solar interior, possibly a non-axisymmetric component of the solar magnetic field (e.g. Stix, 1974; Balthasar and Schüssler, 1983; Ruzmaikin et al., 2001). Analysis of the lowest-order non-axisymmetric modes of the solar magnetic field using WSO synoptic maps also resulted in the detection of a 27.03-day periodicity (Ruzmaikin et al., 2001). Assuming the observed periodicity relates to a distinct solar rotation rate does not aid in constraining the signal source to a unique solar latitude or interior depth. The equatorial rotation rate periods for magnetic tracers have a range of values from 26.4 days for young sunspots (Zappalà and Zuccarello, 1991) to 27.1 days for large area sunspots (Howard, Gilman, and Gilman, 1984). For a thorough review of solar differential rotation measurements see Beck (1999).

Previous studies of photospheric synoptic maps have revealed that active regions are not distributed randomly, but tend to form “complexes of activity” (e.g. Bumba and Howard, 1965; Gaizauskas et al., 1983; Brouwer and Zwaan, 1990). In addition, the longitudinal distribution of major solar flares has been shown to concentrate in active zones (Bai, 1987). Recently, de Toma et al. (2000) used NSO Kitt Peak Vacuum Telescope (KPVT) magnetic synoptic maps to argue that observed persistent bands of active “nests” supports a stable pattern for sources of flux emerging in the tachocline. They determined that these active nests can persist up to seven solar rotations. In our study, we

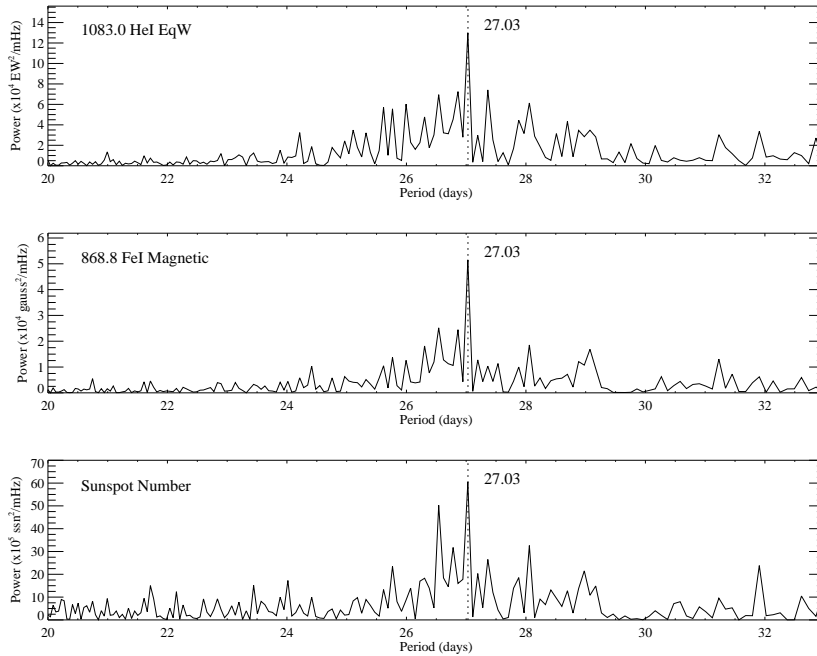


Figure 1. Comparison of power spectra between the KPVT 1083.0 nm He I equivalent width (top), 868.8 nm Fe I unsigned magnetic flux (middle) full-disk integrated time series, and the international sunspot number (bottom) time series. Each time series is sampled at a cadence of 1 day and for the same 8839 day interval (1977.2 to 2001.4, in units of fractional years). The vertical dotted line delineates the 27.03-day period position.

investigate possible signal sources that last for more than two hundred solar rotations. To address the nature of the 27.03-day period signal, and the possibility of a fixed or quasi-stable longitudinal solar structure, the phase coherency of solar surface magnetic activity is investigated using KPVT synoptic data. In particular, we utilize the phase variance of signals from integrated full-disk solar images as a measure of coherence. To localize the solar surface source of the signal, we use spectral analysis of temporally sampled KPVT magnetic synoptic maps. Additionally, to better understand the longevity of 27.0-day period signal, the power and phase coherence are analyzed of the international sunspot number time series for the past 120 years.

2. Integrated Full-Disk Time Series Analysis

The KPVT integrated full-disk time series used to create the power spectra shown in Figure 1 are disk averages of 1 arc-second pixel solar

images of the line-of-sight component of unsigned magnetic flux and the line equivalent width derived from the 868.8 nm Fe I and 1083.0 nm He I lines respectively. At a cadence of one day, the signal coverage for the magnetic and the equivalent width time series are approximately 70% and 61% respectively for the 8839 day interval, from 1977.2 to 2001.4 (fractional years), used to create the spectra in Figure 1. After the temporal gaps are filled with a high-order autoregressive model (e.g. Proakis and Manolakis, 1996), each time series is temporally filtered using a non-recursive digital filter with a band pass with periods between 10 and 60 days. We found that the time series gap filling has a negligible effect on the final calculated power spectra and is used here only to simplify the temporal filtering.

Besides the power spectra for the magnetic and equivalent width time series, the power spectrum of the international sunspot number, from <http://sidc.oma.be>, for the same period is also included in Figure 1. The three power spectra have similar features, including a significant band of power between 25.0 to 29.5 days. Previously observed signals at periods of 28- and 29-days (e.g. Svalgaard and Wilcox, 1975; Sheeley and DeVore, 1986) are clearly evident in the three spectra, most especially in the magnetic data. Also, even though the signal-to-background ratio of the sunspot number spectrum is lower relative to the other two time series, the 27.03-day period signal is notably evident in each of the three spectra. Even with the low spectral resolution, the strength and narrowness of the power implies a coherent signal. However, a large amplitude signal with moderate phase coherence can result in a higher power spectrum signal relative to a smaller amplitude signal with higher coherence (see example in the appendix). To better understand the nature of the 27.03-day period signal coherency, the phase variance of the signal is analyzed in the following subsection.

2.1. SIGNAL COHERENCY

A fixed frequency harmonic signal is defined to be coherent for an interval of a time series investigated if the signal has a negligible temporal variance in phase. One method to estimate a signal's phase is to calculate the instantaneous phase and frequency for each time step over the length of a time series using the analytical signal from the Hilbert transform (e.g. Bracewell, 1985). However, the 27.0-day signal observed in the three time series shown in Figure 1 is in a crowded region of the power spectrum, and the Hilbert transform works best with an isolated narrow band signal. Additionally, wavelet analysis may also give confusing results in crowded spectra.

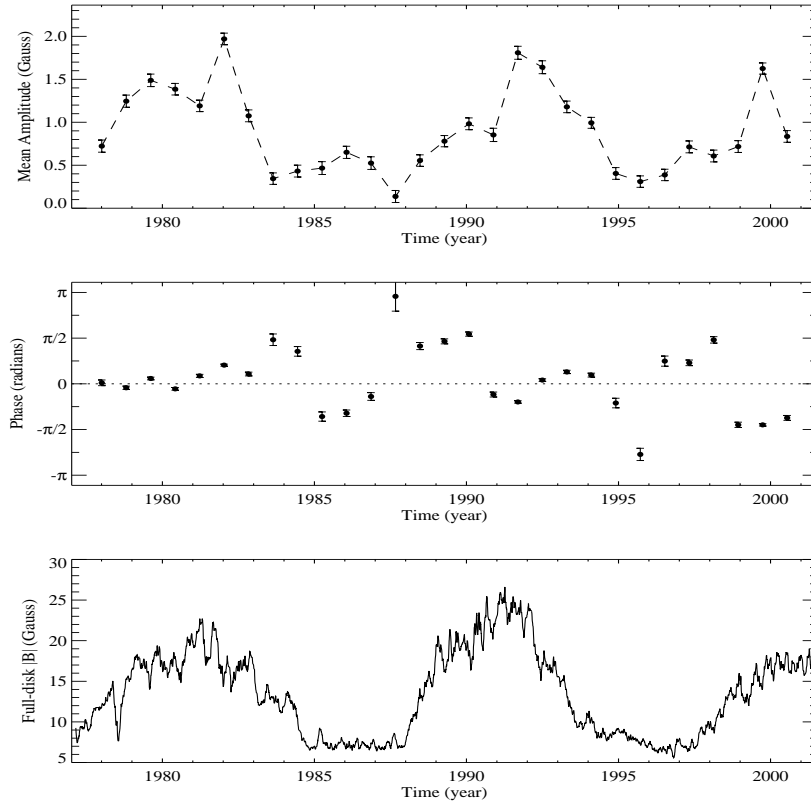


Figure 2. The estimated mean amplitude (top) and zero-mean phase (middle) of the unsigned integrated full-disk magnetic field time series. The amplitude and phase values are for 29 segments with 50% overlap over the same 8839 day interval as in Figure 1. The values are from a non-linear least-squares fit of a cosine function to each segment using a fixed frequency with a period of 27.03 days. In addition, the “raw” integrated full-disk field strength, smoothed with a 27-day window, is displayed for the same period (bottom). The superimposed error bars on the mean amplitude and zero-mean phase values are the $1\text{-}\sigma$ fitting errors.

Instead of using a Hilbert transform type analysis, we estimate the phase and amplitude of a signal from a non-linear least-squares fit of a fixed frequency cosine function for overlapping segments of a time series. As with the power spectra analyses, the time series are gap filled with a high-order autoregressive model and temporally filtered using a non-recursive digital filter with a band pass with periods between 10 and 60 days. No further processing is done to the data before or after the time series is segmented. The time steps that contain gap filled values are given weights of zero during the non-linear least-squares fit of each segment.

In Figure 2, the temporal variation of phase and mean amplitude for the same 8839 day interval as shown in Figure 1, using 29 segments of 589-day duration with 50% overlap, are depicted for the KPVT integrated full-disk magnetic field strength time series using a fixed frequency with a period of 27.03 days. The phase is displayed relative to the error weighted mean phase, where the errors are from the fit. The signal is mostly coherent during periods of large amplitude. Note, however that the signal, though coherent, is approximately 90 degrees out of phase relative to the error weighted mean phase for the maximum period from year 1999.5 to 2001. As expected, the signal mean amplitude extremes correspond reasonably well with high amplitudes of the integrated full-disk magnetic time series shown in Figure 2. For this 24 year interval the 27.03-day period signal phase variance is minimum, i.e. more coherent, during maximum solar magnetic activity. Also, note that the signal’s phase wanders approximately ± 90 degrees during lower activity spans. The question of how the phase variance of this signal compares to other frequencies is addressed in the following subsection.

2.1.1. *Phase Coherence Spectrum*

As a measure of a signal’s coherency, relative to neighboring frequencies, the inverse phase variance of a segmented time series for fixed frequencies within a selected frequency window is used to create a “phase coherence spectrum” (PCS). The basic premise of the PCS is that long-lived coherent signals will have a smaller phase variance than shorter lived or less coherent signals relative to the time series duration investigated. To create the PCS, the phase and amplitude are estimated from a non-linear least-squares fit of a fixed frequency cosine function to each time series segment. Next, the temporal variation of the phase and amplitude are quantified for a discrete frequency and segment length. The phase coherence is defined here to be the inverse phase variance, where the mean phase and the phase variance are weighted by the inverse of the phase error determined from the non-linear least squares fit. The chosen segment length will affect the variance of the estimated phase values. As the segment length increases the temporal phase discontinuities approach the value of the mean phase for the time series interval. The nature and attributes of the PCS, along with the effects of varying the segment length, are explored in more detail in the appendix.

The PCS method is similar to the phase dispersion minimization (PDM) method (Stellingwerf, 1978). The PDM method folds a given time series into phase bins for a selected period, then the variances of the binned values are compared for the chosen frequency band to select

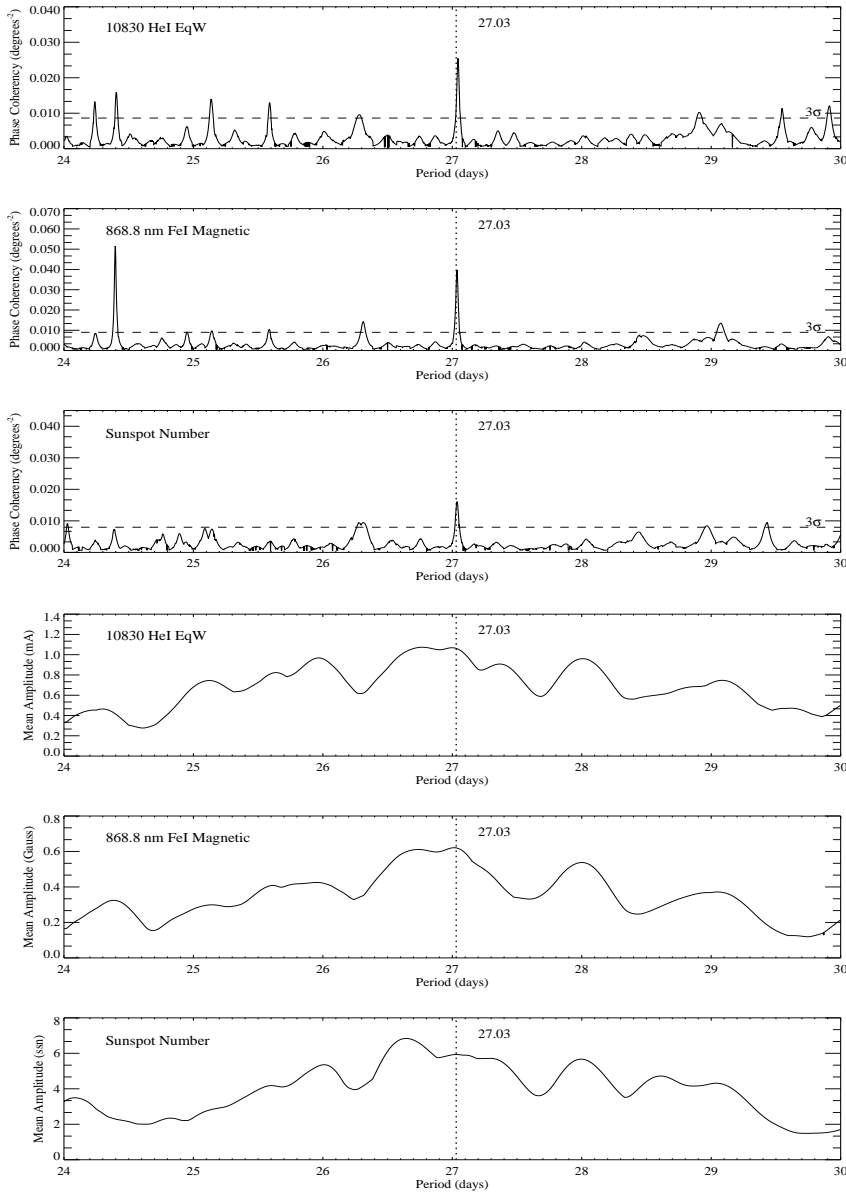


Figure 3. Phase coherence spectra (top three) and the error weighted mean amplitude spectra (bottom three) for the KPVT integrated full-disk 1083.0 nm He I equivalent width, 868.8 nm Fe I unsigned magnetic flux time series, and the sunspot number time series for the same 8839 day interval used in Figure 1. The PCS were created using 9 segments with 50% overlap and widths of 1/5 the total time series duration. The vertical dotted line delineates the 27.03 day period position. The horizontal dashed line indicates the 3- σ noise level.

out those periods that correspond to periodic signals. However, unlike the PDM method, the PCS method estimates and utilizes the temporal variation of phase and amplitude, along with the fitting errors, for a given frequency. The temporal error information is critical for analyzing long lived signals that may have “dormant” states, i.e. periods when there is a very small or no signal amplitude observed relative to other segments of a time series, e.g. solar magnetic activity (see Figure 2).

The phase coherence and mean amplitude spectra for the magnetic, equivalent width and sunspot number time series are shown in Figure 3. All three spectra are from the same 8839 day interval as in Figures 1 and 2. An example of the usefulness of the phase coherence and mean amplitude spectra is illustrated with the 28.1-day and 29.0-day period signals which are evident in the power spectra in Figure 1. From Figure 3, the lack of phase coherence and the increased mean amplitude at a period of 28 days implies that the signal is primarily the result of strong magnetic field regions incoherently distributed relative to a weaker but more spatially coherent source of the 29.0-day signal.

As with the power spectra in Figure 1, the 27.03-day period signal is notable in each of the phase coherence spectra shown in Figure 3. Within the frequency band between 25 and 29 days, the 27.03-day period signal is clearly the most coherent. At this stage, we confirm the results of Neugebauer et al. (2000). The highest coherence peak within the magnetic PCS is at a period of 24.4 days. This coherence spike is most likely a spurious signal because it is not equally coherent in the sunspot and 1083 PCS relative to the 27.03-day period signal. Another signal of interest, albeit marginally detected, is at a period of 26.3 days. This period of rotation is faster than any measured magnetic surface tracer. However, this signal may be related to young sunspots which have a measured rotational period of 26.37 days at the equator (Zappalà and Zuccarello, 1991). Additionally, the maximum mean amplitude within the 24 to 30 day period band is near or at a period of 27.0 days in each of the mean amplitude spectra. With clear evidence for a coherent solar surface magnetic signal in Figures 1 and 3, the next step is to better understand the character of the signal source. In the following section, the solar surface is investigated for regions with coherently reoccurring magnetic activity during the past two solar cycles that may account for the 27.03-day period signal.

3. Spatially Resolved Time Series Analysis

To explore if any particular solar surface region is a probable source of the 27.03-day signal, nearly 24 years of the KPVT unsigned pho-

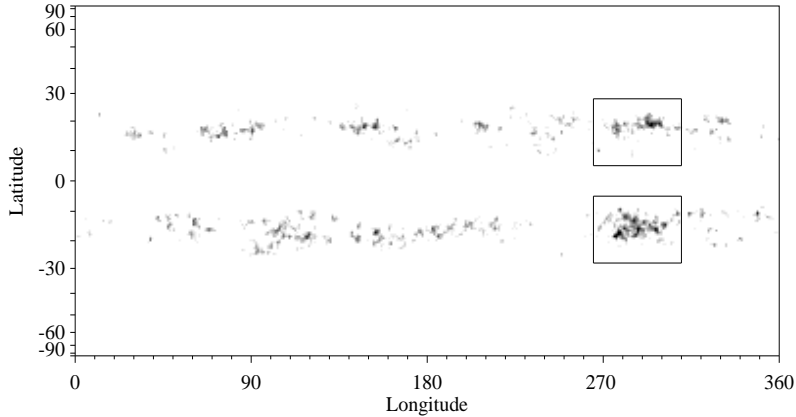


Figure 4. The average of 330 unsigned magnetic flux synoptic maps using a rotation period of $27.03 \pm .02$ days. The maps are from KPVT observations during years 1977.70 through 2001.34 (Carrington rotations 1645 through 1974). Regions between white and black are between $2\text{-}\sigma$ and $4\text{-}\sigma$ above the mean respectively. Longitude values are relative to Carrington rotation 1645. The two primary complexes of magnetic activity are highlighted by the boxed regions.

ospheric magnetic flux synoptic maps are averaged using a rotational period of 27.03 days. The KPVT synoptic maps used here are described by Harvey et al. (1980), and also see de Toma et al. (2000). Shifting each synoptic map relative to the previous maps using a rotation period of $27.03 \pm .02$ days, reveals two long-lived complexes of activity exhibited in Figure 4. The two stronger-than-average regions of magnetic activity (boxed areas) are nearly aligned at 290 degrees longitude, one on each hemisphere, in the Carrington Rotation number 1645 reference frame. The alignment in longitude of the two complexes of activity is suggestive of a fixed magnetic sector structure. However, when the synoptic maps are averaged over shorter periods, shown in Figure 5, the boxed regions do not reveal persistent activity relative to other longitudes. The two boxed regions highlighted in Figure 4 are primarily the result of strong activity during solar cycle 21 (between 1986 and 1996), displayed in Figure 5.

In addition to averaging synoptic maps with a 27.03-day rotational period, the synoptic maps were temporally sampled to create latitudinal time series for spectral analysis. For this analysis the unsigned magnetic flux synoptic maps are binned in latitude and longitude. As with the integrated full-disk spectral analysis, temporal gaps are filled with a high-order autoregressive model, and each time series is temporally filtered using a non-recursive digital filter with a band pass between 10 and 60 days. The power spectra for middle to low latitudes

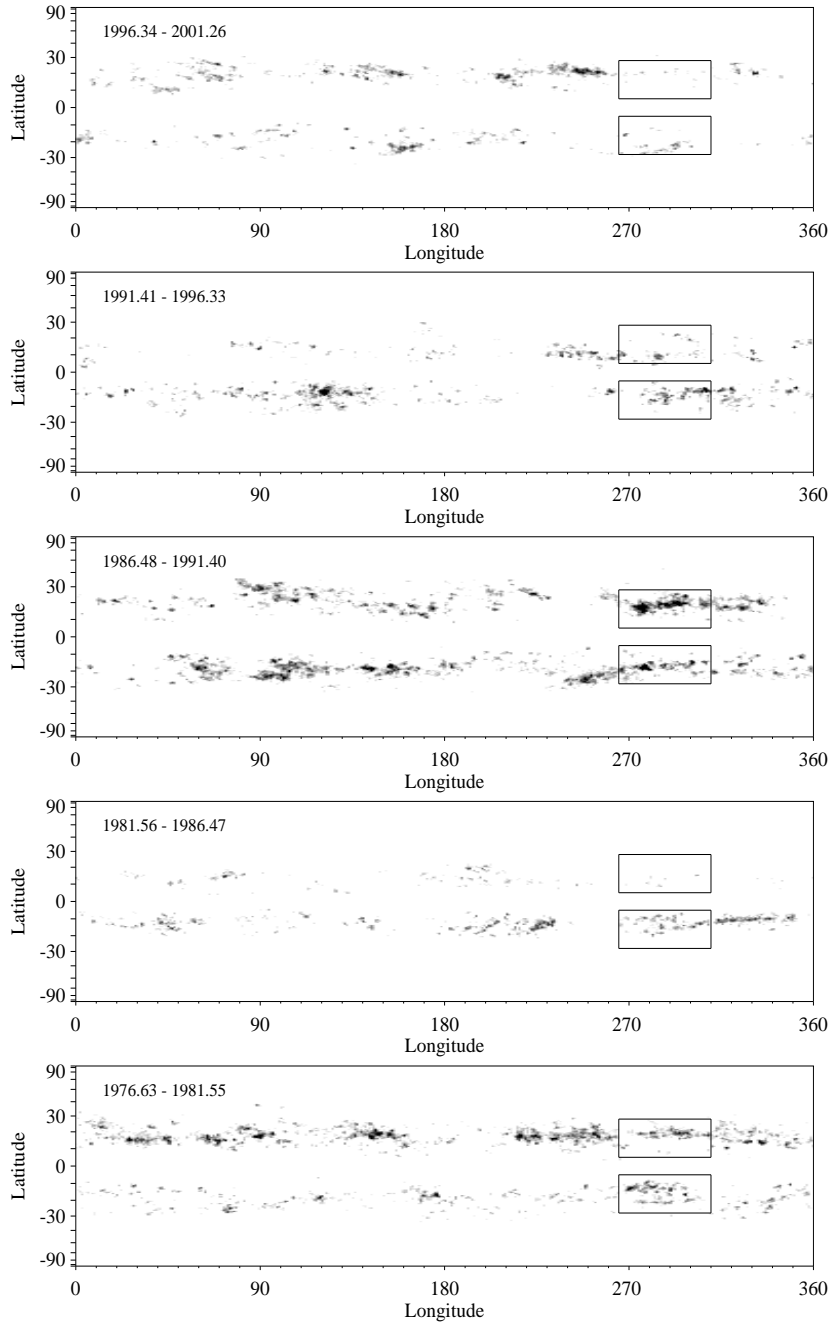


Figure 5. Averages of sets of 66 unsigned magnetic flux synoptic maps using a rotation period of $27.03 \pm .02$ days. Regions between white and black are between $2\text{-}\sigma$ and $6\text{-}\sigma$ above the average mean of the five averaged maps respectively. Longitude values are relative to Carrington rotation 1645. The two boxed regions in each image corresponds to the highlighted regions in Figure 4.

are displayed in Figure 6. As expected from long-term sunspot observations, the lower and higher latitudes contribute negligible power to the integrated full-disk power spectrum.

From Figure 6, it is evident that the 27.03-day period signal is distinctly from the northern hemisphere. Additionally, the ~ 28 -day signal is predominantly from the southern hemisphere. These results support the previous findings of asymmetric rotation periods for the solar hemispheres, 26.9 ± 0.2 and 28.1 ± 0.2 days for the northern and southern respectively, reported by Hoeksema and Scherrer (1987) and Antonucci, Hoeksema, and Scherrer (1990). From Figure 4, the maximum amplitude in the northern hemisphere complex is at a latitude of 18 ± 2 degrees. This result agrees with the finding by Antonucci, Hoeksema, and Scherrer (1990) that the 26.9-day period signal source is centered at a latitude of 15 degrees north, covering a latitude zone of approximately 24 degrees wide. At a latitude of 18 degrees, the 27.03-day period signal is consistent with the solar interior rotation rate of 27.06 days at a depth of $0.95 R_{\odot}$, obtained from helioseismic studies using data from the Michelson Doppler Imager (Schou et al., 1998).

4. Signal Longevity

To estimate the longevity of the 27.03-day period signal, we analyzed more than 120 years of the international sunspot number time series. Previously, Bogart (1982) found evidence for preferred activity longitudes using spectral analysis of the sunspot number time series. The length and generally consistent character of the sunspot number time series, both in quality and cadence, makes it ideal for testing the long-term persistent nature of a particular signal. Furthermore, the sunspot number time series is of interest since its power spectrum shown in Figure 1 is remarkably similar to the KPVT spectra and therefore appears to be useful as a proxy for past solar surface magnetic activity.

In addition to the sunspot number power spectra for the most recent 24 year interval displayed in Figure 1, spectra for four additional periods of equal length during the past 120 years are exhibited in Figure 7. Using the same time series analysis method as discussed in section 2, the 27.03-day period signal is not found to be significant in the power spectra for the years between 1880 and 1977 as compared to the 1977 to 2001 spectrum. The only frequency to have notable power in more than one of the five intervals is at a period of approximately 27.5 days during years 1904 through 1977 (see the top three graphs in Figure 7).

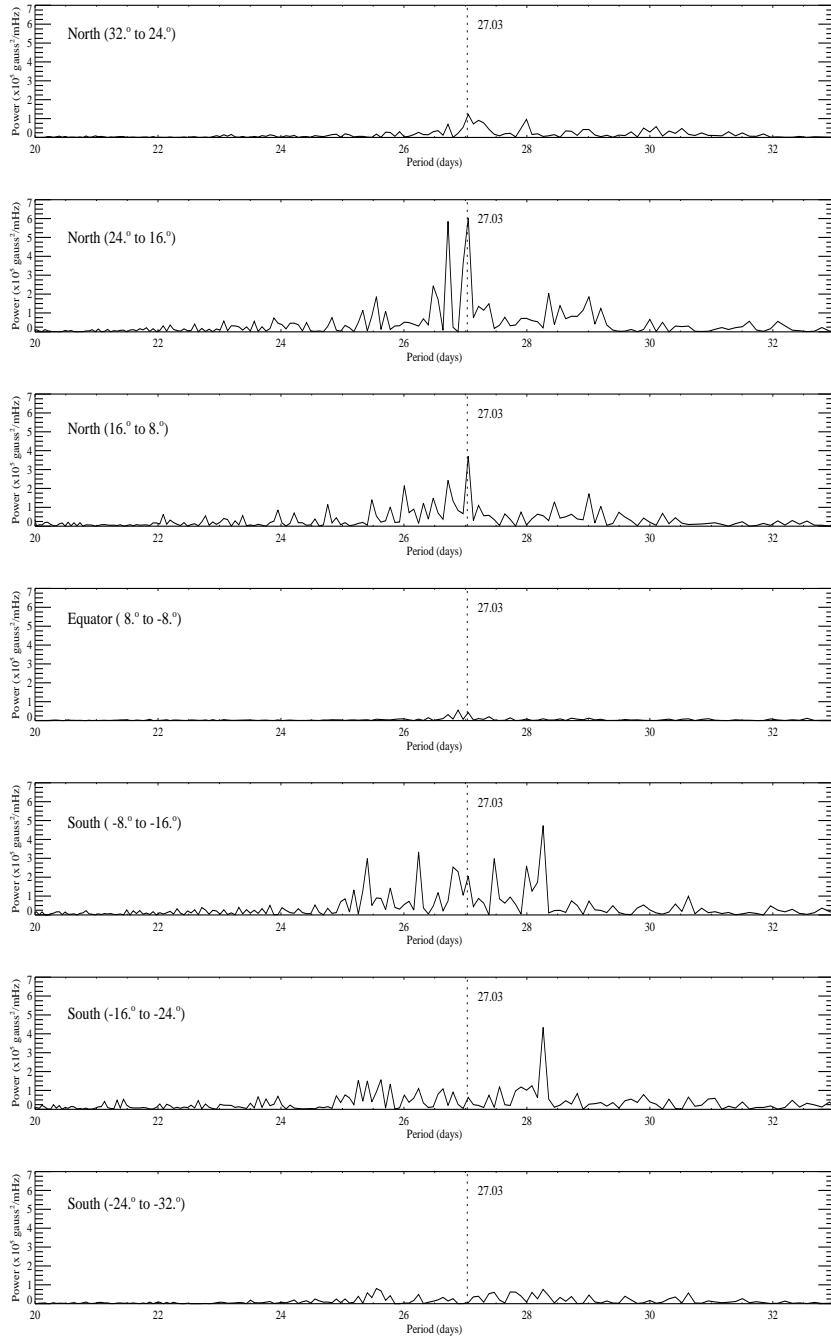


Figure 6. Comparison of power spectra for northern (top three), equatorial (center), and southern (bottom three) latitude bands from 330 unsigned magnetic synoptic maps for the same period used to create the average synoptic maps in Figures 4 and 5. The vertical dotted line delineates the 27.03 day period position.

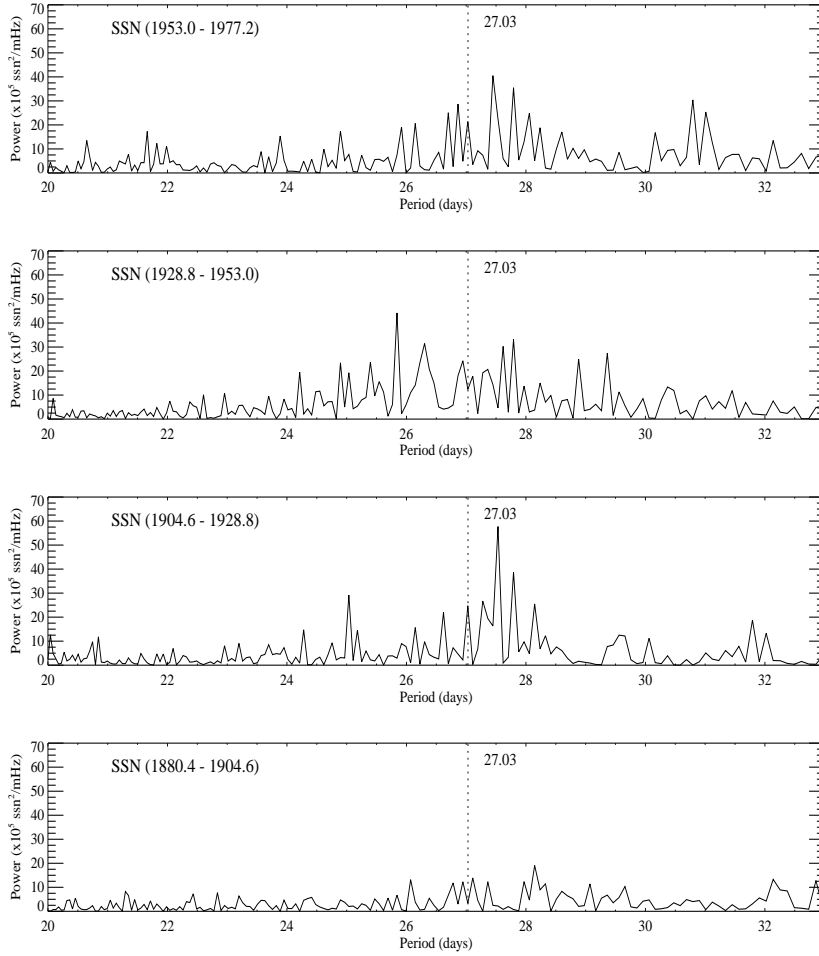


Figure 7. The international sunspot number (SSN) power spectra for four consecutive periods during the past 120 years. The time series cadence of 1-day and interval length of 8839-days used for each power spectrum is equivalent to those of the comparison in Figure 1. The interval values for each time series (in parentheses) are in fractional years. The vertical dotted line delineates the 27.03 day period position.

The phase coherence and mean amplitude spectra are revealed in Figures 8 and 9 respectively. Again, the 27.03-day period signal is found to be insignificant for the years between 1880 and 1977. In Figure 8, the 27.5-day period signal has marginally significant phase coherence during the intervals 1904-1928 and 1953-1977. Nonetheless, the maximum mean amplitude is centered on a period of 27.5 days between years 1904 and 1977 (top three plots in Figure 9). This corresponds to the persistent 27.5 ± 0.5 -day period signal reported by Bogart (1982).

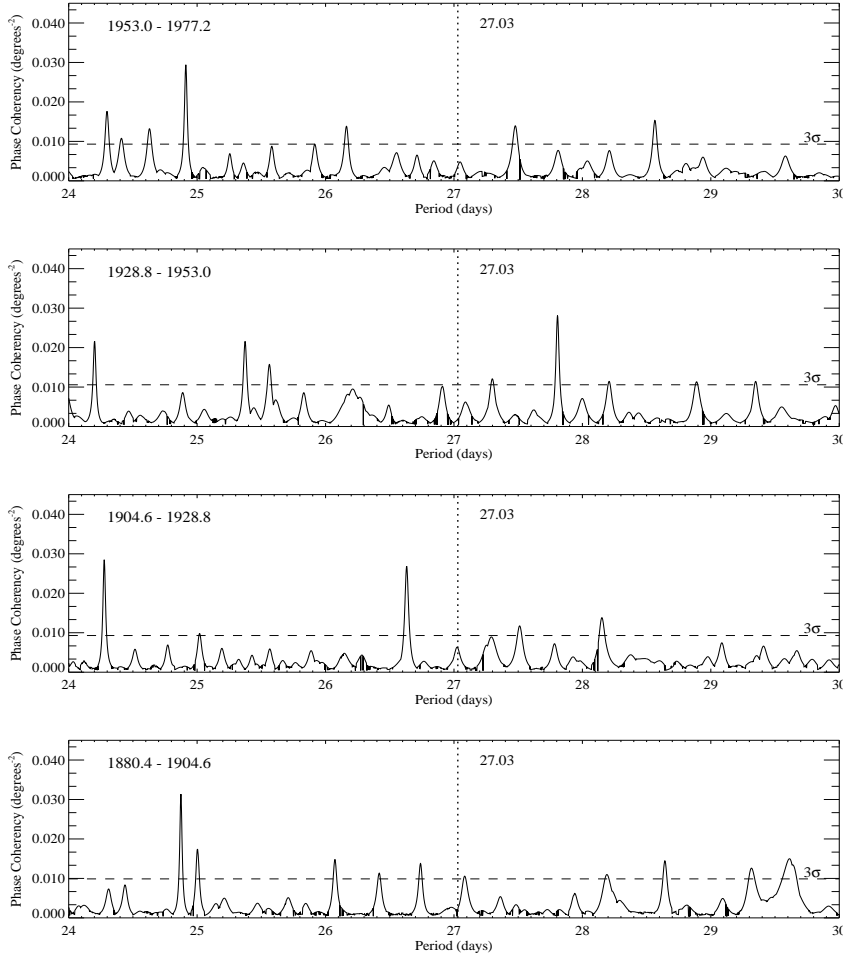


Figure 8. The phase coherence spectra for the sunspot number time series over the past 120 years, using 9 segments with 50% overlap and widths of $1/5$ the total time series length. Each time series has the same 1-day cadence and interval length of 8839-days as used for those in Figure 1. The vertical dotted line delineates the 27.03 day period position. The horizontal dashed line indicates the $3\text{-}\sigma$ noise level.

Other than the 27.5-day period signal, no other frequency is found to have notable coherence during the past 120 years. However, the signal-to-background ratio (S/B) of the sunspot number power spectra in Figure 1 is lower than that of the magnetic or 1083 spectra. Likewise, the phase coherence in Figure 3 of the sunspot number time series is significantly lower than in the other two time series. The poor S/B and lack of coherence may be reflective of the sunspot number time series, i.e. ambiguity in the scaling used to calculate the sunspot number value,

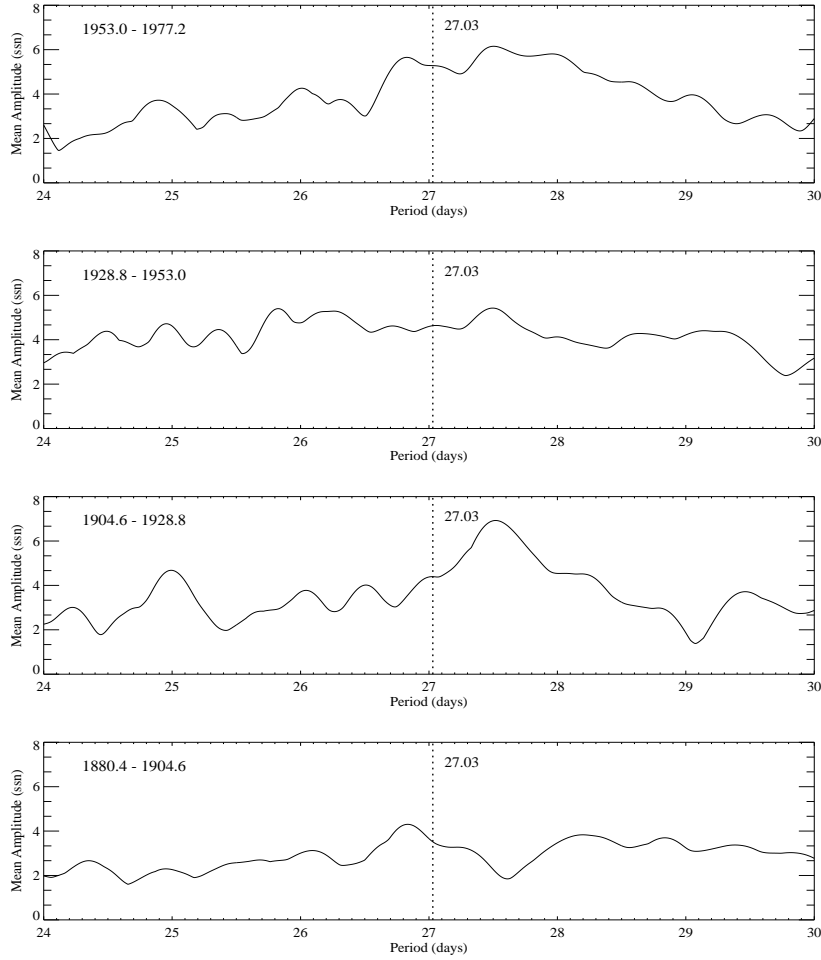


Figure 9. The error weighted mean amplitude for the international sunspot number time series during the past 120 years, using 9 segments with 50% overlap and widths of $1/5$ the total time series span. Each time series has the same 1-day cadence and interval length of 8839-days as used for those in Figure 1. The vertical dotted line delineates the 27.03 day period position.

or because sunspots last for a shorter time than the plages seen in the magnetic and 1083 equivalent width data.

5. Conclusions

A strong 27.03-day period signal, initially reported by Neugebauer et al. (2000), is clearly detected in over two decades of full-disk KPVT photospheric magnetic flux synoptic data. Using phase coherence analysis,

the coherency of the 27.03-day signal is found to be significant, relative to neighboring periods, for the past two decades. The signal is notably coherent during periods when the signal amplitude is large for the past 24 year term. From analysis of spatially-resolved KPVT magnetic flux synoptic maps, the origin of the 27.03-day period signal is found to be long-lived complexes of activity in the northern hemisphere at a latitude of approximately 18 degrees. These quasi-stationary magnetic patterns may be the result of a flux transport phenomenon, e.g. the model proposed by Sheeley, Nash, and Wang (1987) where the rotational shear of magnetic flux is offset by supergranular transport and the meridional flow. Additionally, the marginal pattern coherence could be produced by organized emergence of flux due to a quasi-stable interior structure related to the solar dynamo (e.g. Ruzmaikin, 1998; Ruzmaikin, 2000). A detailed analysis of magnetic activity, during the past 24 years within a latitude band of a few degrees centered on 18 degrees, using individual magnetograms instead of synoptic maps would help clarify the signal source, i.e. young sunspots verses small area sunspots.

However, the 27.03-day signal lacks clear coherence in the international sunspot number time series for the period from 1880 to 1977. The signal with the greatest longevity during most of the interval 1904 through 1977 is at a period of 27.5 days. This 27.5-day periodicity, though not particularly coherent, corresponds to a rotation rate that is typically observed for the latitude bands associated with sunspot activity. There is no evidence for a long-lived (more than three 11-year solar cycles) phase coherent signal that would indicate a permanent solar magnetic non-axisymmetric component at a fixed solar interior depth.

6. Acknowledgments

This research was supported in part by the Office of Naval Research Grant N00014-91-J-1040. The NSO-Kitt Peak data used here are produced cooperatively by NSF/AURA, NASA/GSFC, and NOAA/SEC.

Appendix

The “phase coherence spectrum” (PCS) is created by estimating the phase and amplitude for each segment span of a segmented time series at fixed frequencies within a chosen frequency band window. From a non-linear least-squares fit to a cosine function of the form $f_i(t) = a_i \cos(\omega t + \phi_i)$, the amplitude, a_i , and phase, ϕ_i , are estimated for each

time series segment i , where ω and t are the cyclic frequency and time index respectively. The phase coherence at a given frequency ω , over the full length of a time series, is defined here as

$$\Phi_{\text{coh}}(\omega) = \frac{1}{\sigma_{\text{phase}}^2}, \quad (1)$$

where σ_{phase}^2 is the error weighted phase variance, defined as

$$\sigma_{\text{phase}}^2 = \frac{\sum_{i=1}^N [(\phi_i - \bar{\phi})^2 w_i]}{(N-1) \sum_{i=1}^N w_i}. \quad (2)$$

The total number of segments is represented by N . The mean phase and phase variance are weighted by the inverse of the phase error, $w = 1/\sigma_{\phi}^2$, determined from the non-linear least squares fit. One key caveat when calculating the PCS is to sift the estimated phase values to within $\pm\pi$ of the error weighted mean phase of all the segments. This is accomplished by adding $\pm 2\pi$ to each phase value, which by the character of its definition is constrained by mod 2π , to minimize the error weighted phase variance. However, due to the cyclic nature of the phase, the phase time series for a given frequency will have spurious discontinuities. An example of this is illustrated in the phase time series shown in Figure 2 (middle graph) near year 1995.

A pure sine or cosine signal that remains in phase over the length of a time series, and with no noise, would have a phase coherence value (from Equation 1) of infinity. However, this unconstrained upper limit is not a problem with a time series that includes noise. Nonetheless, if a signal of interest is sinusoidal and nearly noise free, the phase variance values from Equation 2 can be employed instead of the phase coherence. The phase coherency lower limit is constrained by the maximum variance allowed after the phase sifting process. The lower limit can be estimated from Equations 1 and 2 by assuming an equal number of segments have phases that are either 90 or -90 degrees from the mean, with equal error weights for each segment. For a given time series realization it is possible to have spurious high phase coherent signals. Unless clearly associated with features detected in the power spectrum, these spurious signals are noticeably narrower than a PCS signal. One method to improve the signal-to-background ratio of the estimated PCS is by averaging the PCS calculated using various segmentation lengths.

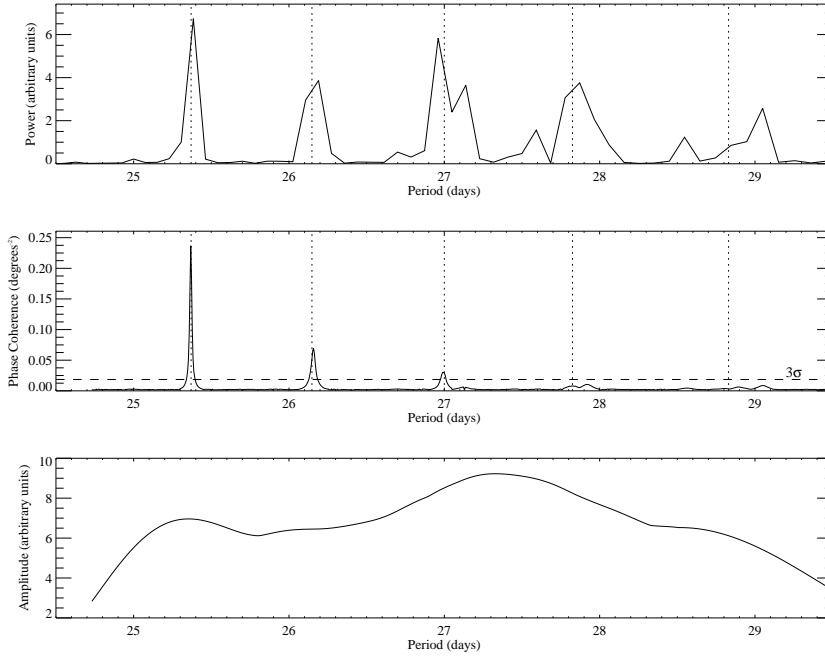


Figure 10. The power (top), phase coherence (middle), and the mean amplitude (bottom) spectra for a given realization of a simulated time series. The time series includes five signals with coherencies, left to right, 100%, 80%, 60%, 40%, 20%, and unit-less excitation amplitudes of 5, 5, 10, 10, 10 respectively. The PCS was created using 21 segments with 50% overlap and widths of 1/11 the total time series span. The vertical dotted lines delineate the frequency of the simulated signal. The horizontal dashed line in the phase coherence spectrum (middle) indicates the $3\text{-}\sigma$ noise level.

An example power spectrum, phase coherence spectrum, and mean amplitude spectrum for a single realization of a simulated time series are shown in Figure 10. The simulated time series is 8250 days in length, with 1 day cadence, and includes five signals with coherencies of 100%, 80%, 60%, 40%, 20% and unit-less excitation amplitudes of 5, 5, 10, 10, 10 respectively. The coherency percentage is defined here, albeit arbitrarily, by dividing the simulated time series interval into five segments, where in-phase segments for a given signal are excited with a relative phase of zero. The out-of-phase segments are excited to have a phase with a mean absolute difference of approximately 100 degrees relative to the mean phase of the time series interval. The Gaussian white noise added to the simulated time series is scaled in amplitude such that the 60% coherent signal has a S/B of 6.4 estimated from the distribution of signal fits to the power spectrum.

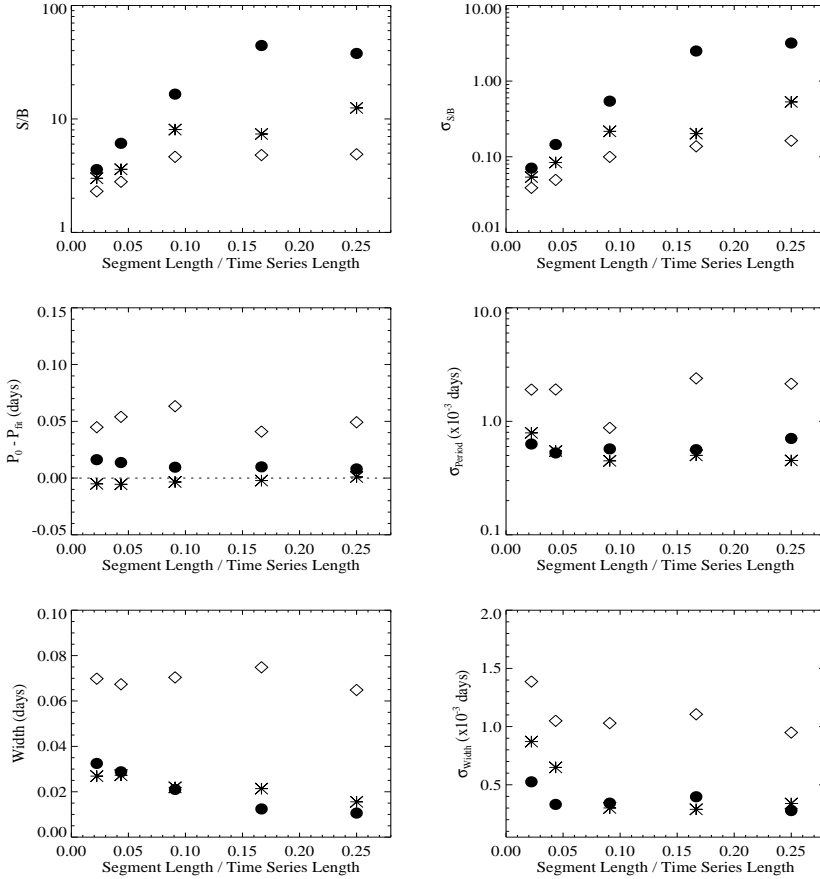


Figure 11. The phase coherence signal-to-background ratio (S/B), residual of the difference between the true and the fitted signal period, and the fitted Gaussian full-width as a function of segment length. The values are from spectra using a simulated time series with three signals differing only by phase coherence percentage over the length of the time series: 80% (solid circles), 60% (stars), 40% (open triangles), and unit-less excitation amplitudes of 5, 10, 10 respectively. The left-hand column displays the mean S/B , signal period and width estimates of 500 realizations at each segmentation length position. The right-hand column depicts the standard deviations of the distributions of the estimated parameters. The horizontal dotted line, in the middle left-hand column plot, delineates the simulated signal position.

The power spectrum in Figure 10 was created using the same time series analysis method as discussed in section 2. Note that from the power spectrum it is unclear if the 60% and 40% coherence signals are more or less coherent than the 80% coherence signal, whereas the PCS gives some indication of the relative coherence. Also, note the narrowness and broadness of the phase coherence and mean amplitude

signals respectively in Figure 10. The narrowness, or sensitivity, of phase coherence signal is partly due to the estimation of the phase within the cosine function, whereas the amplitude signal is broad as a result of being a multiplicative term in the non-linear least-squares fit. Though the resolution of the PCS is arbitrary, to account for the narrowness of phase coherence signal, a factor of ten or greater in frequency resolution than would be used in a given frequency band with standard fast Fourier analysis is a convenient exploratory resolution.

The phase coherence analysis stability of the simulated time series is illustrated by the Monte Carlo simulation results shown in Figure 11. These PCS results are derived from Gaussian fits, for 500 realizations, to the inner three signals with coherencies of 80%, 60%, and 40%, illustrated for one realization in Figure 10. The left-hand column of the figure displays the mean signal-to-background ratio (S/B), signal period and width estimates of 500 realizations at each segmentation length position. The right-hand column shows a measure of the random errors using the standard deviations of the distributions of the estimated parameters. As indicated in Figure 11, the PCS signal-to-background ratio decreases with shorter segment lengths due to fewer cycles of the given period being fitted, in addition to the growing influence of the shorter lived coherent signals and the background. A segmentation overlap of 50% is used in all of the time series PCS analysis done in this paper. With overlapping segments, the temporal resolution is improved while preserving the signal sampling used for the non-linear least-squares fit. Also highlighted in Figure 11 are the limitations of detecting signals that are marginally coherent over an interval analyzed. The S/B of the 40% coherence signal is notably lower in value relative to the 60% and 80% coherence signal values. Also, the measured frequency position for the 40% coherence signal is systematically offset from the true value, along with a broader fitted signal width. Nonetheless, the Monte Carlo results demonstrate that the phase coherence spectrum is a beneficial complement to power spectrum analysis as a measure of the relative phase coherence for signals under investigation.

References

- Antonucci, E., Hoeksema, J. T., and Scherrer, P. H.: 1990, *Astrophys. J.*, **360**, 296.
 Bai, T.: 1987, *Astrophys. J.*, **314**, 795.
 Bai, T.: 1990, *Astrophys. J.*, **364**, L17.
 Balthasar, H., and Schüssler, M.: 1983, *Solar Phys.*, **87**, 23.
 Beck, J. G.: 1999, *Solar Phys.*, **191**, 47.
 Bogart, R. S.: 1982, *Solar Phys.*, **76**, 155.

- Bracewell, R. N.: 1985, *Aust. J. Phys.*, **38**, 1009.
- Brouwer, M. P., and Zwaan, C.: 1990, *Solar Phys.*, **129**, 221.
- Bumba, V., and Howard, R.: 1965, *Astrophys. J.*, **141**, 1502.
- de Toma, G., White, O. R., and Harvey, K. L.: 2000, *Astrophys. J.*, **529**, 1101.
- Gaizauskas, V., Harvey, K. L., Harvey, J. W., and Zwaan, C.: 1983, *Astrophys. J.*, **265**, 1056.
- Gosling, J. T., Asbridge, J. R., Bame, S. J., and Feldman, W. C.: 1977 *J. Geophys. Res.*, **82**, 2371.
- Harvey, J. Gillespie, B., Meidaner, P., and Slaughter, C.: 1980, World Data Center A Report UAG-77.
- Hoeksema, J. T., and Scherrer, P. H.: 1987, *Astrophys. J.*, **318**, 428.
- Howard, R., Gilman, P. A., and Gilman, P. I.: 1984, *Astrophys. J.*, **283**, 373.
- Neugebauer, M., Smith, E. J., Ruzmaikin, A., Feynman, J., and Vaughan, A. H.: 2000, *J. Geophys. Res.*, **105**, A2, 2315.
- Proakis, J. G., and Manolakis, D. G.: 1996, *Digital Signal Processing: Principles, Algorithms, and Applications*, 3rd Ed. (Prentice Hall: Upper Saddle River, NJ), Chapter 11.
- Ruzmaikin, A.: 1998, *Solar Phys.*, **181**, 1.
- Ruzmaikin, A.: 2000, *Solar Phys.*, **192**, 49.
- Ruzmaikin, A., Feynman, J., Neugebauer, M., and Smith, E. J.: 2001, *J. Geophys. Res.*, **106**, A5, 8363.
- Schou, J., Antia, H. M., Basu, S., Bogart, R. S., Bush, R. I., Chitre, S. M., Christensen-Dalsgaard, J., Di Mauro, M. P., Dziembowski, W. A., Eff-Darwich, A., Gough, D. O., Haber, D. A., Hoeksema, J. T., Howe, R., Korzennik, S. G., Kosovichev, A. G., Larsen, R. M., Pijpers, F. P., Scherrer, P. H., Sekii, T., Tarbell, T. D., Title, A. M., Thompson, M. J., and Toomre, J.: 1998 *Astrophys. J.*, **505**, 390.
- Sheeley, N. R., Jr., and DeVore, C. R.: 1986, *Solar Phys.*, **104**, 425.
- Sheeley, N. R., Jr., Nash, A. G., and Wang, Y.-M.: 1987, *Astrophys. J.*, **319**, 481.
- Stellingwerf, R. F.: 1978, *Astrophys. J.*, **224**, 953.
- Stix, M.: 1974, *Astron. Astrophys.*, **37**, 121.
- Svalgaard, L., and Wilcox, J. M.: 1975, *Solar Phys.*, **41**, 461.
- Zappalà, R. A., and Zuccarello, F.: 1991, *Astron. Astrophys.*, **242**, 480.

